Environmental Science & Technology

Article

pubs.acs.org/est

Comparative toxicity of nanoparticulate/bulk Yb_2O_3 and $YbCl_3$ to cucumber (*Cucumis sativus*)

Peng Zhang,[†,†] Yuhui Ma,[†,†] Zhiyong Zhang,[†,*] Xiao He,[†] Zhi Guo,[‡] Renzhong Tai,[‡] Yayun Ding,[†] Yuliang Zhao,[†] and Zhifang Chai[†]

[†]Key Laboratory for Biological Effects of Nanomaterials and Nanosafety, Key Laboratory of Nuclear Analytical Techniques, Institute of High Energy Physics, Chinese Academy of Sciences, Beijing 100049, People's Republic of China;

[‡]Shanghai Synchrotron Radiation Facility, Shanghai Institute of Applied Physics, Chinese Academy of Sciences, Shanghai 201204, People's Republic of China

Supporting Information

ABSTRACT: With the increasing utilization of nanomaterials, there is a growing concern for the potential environmental and health effects of them. To assess the environmental risks of nanomaterials, better knowledge about their fate and toxicity in plants are required. In this work, we compared the phytotoxicity of nanoparticulate Yb_2O_3, bulk Yb_2O_3, and $YbCl_3{\cdot}6H_2O$ to cucumber plants. The distribution and biotransformation of the three materials in plant roots were investigated in situ by TEM, EDS, as well as synchrotron radiation based methods: STXM and NEXAFS. The decrease of biomass was evident at the lowest concentration (0.32 mg/L) when exposed to nano-Yb_2O_3, while at the highest concentration, the most severe inhibition was from $YbCl_3$. The inhibition was dependent on the actual amount of toxic Yb uptake by the cucumber plants. In the intercellular regions of the roots, Yb_2O_3 particles and $YbCl_3$ were all transformed to $YbPO_4$. We speculate that the dissolution of Yb_2O_3 particles induced by the organic acids exuded from roots played an important role in the phytotoxicity. Only under the nano-Yb_2O_3 treatment, $YbPO_4$ deposits were found in the cytoplasm of root cells, so the phytotoxicity might also be attributed to the Yb internalized into the cells.

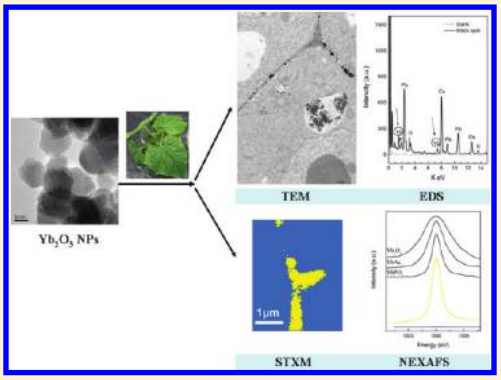

INTRODUCTION

The properties of nanoparticles (NPs) and their increasing application in various commercial products have raised concerns about their environmental fate and possible harmful effects on the ecosystem and human health.[1,2] In order to assess the environmental risks of NPs, better knowledge about their mobility, bioavailability, and ecotoxicity are required.[3,4]

Plants are an important component of the ecological system and may serve as a potential pathway for the transporting of NPs.[5] Through the food chain, NPs might be accumulated in higher-level organisms.[6,7] Phytotoxicity of some types of NPs has been tested by the seed germination and root elongation of several plant species.[8−11] However, the behavior of NPs in plants and the mechanism of toxicity of NPs are still little understood. Given the well-known toxicity of the ionic forms of some heavy metals, it is complicated to understand the effects of NPs because of the coexistence of particles and ionic forms. They will likely exhibit different fate and transport characteristics, and may have independent or synergistic toxicity. Franklin et al. noticed that the toxicity of ZnO NPs was solely due to the dissolved Zn.[12] However, a later study on the phytotoxicity of ZnO NPs to ryegrass indicates that the potential toxicity could not be explained by the dissolution of ZnO NPs alone.[13] The similar cases for other metal and metal oxide NPs have been reported.[14,15] It is not clear whether the toxicity in plants is caused by NPs themselves or their biotransformation outside or inside the plants. Therefore, care needs to be taken in ascribing toxicity to nanoparticles per se when the effects may be related, at least in part, to simple solubility.

With the rapidly increasing applications in various areas of industry and commerce, NPs can be released into the environment intentionally or accidentally. After getting into the environment or biological systems, the toxic effects of NPs will depend not only on the initial properties, but also on the physicochemical evolution in the surroundings.[16] Both abiotic and biological transformations are important for investigating the effects of NPs.[17,18] It is necessary to assess the characteristics of NPs before use, at the moment of delivery, and during interaction with biological environments.[19] In order to unravel the toxicity mechanisms of NPs, many techniques have been used to detect, identify, and understand the composition of NPs in organisms. Transmission electron microscopy (TEM) is most often used to locate and characterize NPs in tissues. Unfortunately, this method could

Received: August 5, 2011
Revised: October 31, 2011
Accepted: December 20, 2011
Published: December 20, 2011

 © 2011 American Chemical Society

not identify the chemical species of the electron-dense deposit in TEM images. Recently, synchrotron X-ray absorption spectroscopy (XAS) has been used to differentiate the chemical species and determine the biotransformation of NPs in plants.[20,21] However, the distribution and in situ chemical information of NPs in samples could not be elucidated through this method because the results came from the homogenized dried tissues by grinding. Synchrotron-based scanning transmission X-ray microscopy (STXM) techniques coupled with near edge X-ray absorption fine structure (NEXAFS) spectroscopy can be used to analyze thin samples in situ with a spatial resolution of better than 30 nm, with no need for prior chemical extraction or staining.[22] On the basis of STXM analyses, different biochemical compounds can be specifically imaged at the nm scale, and information on elemental speciation can be provided by NEXAFS spectra.[23] This methodology has seldom been used to study plant or animal cells in situ due to the lower concentration of elements in the regions of interest.

The rare earth elements (REE) are a group of 15 chemically similar metallic elements. REE oxide nanomaterials are one kind of advanced materials and have extensive applications in the paint coating, polishing powder, luminescent materials, and automobile exhaust purification, etc.[24,25] With wide use, concerns about the environmental fate and potential influence on the ecosystems of these materials were enhanced. Ytterbium oxide (Yb_2O_3) NPs, the representative of heavy REE oxide NPs, are used in luminescent materials, catalysts, etc.[26] We previously found Yb_2O_3 NPs inhibited the root elongation of several plants, but the mechanism was unknown.[11] Here, we assess the toxicity of Yb_2O_3 NPs to a terrestrial plant cucumber (*Cucumis sativus*) in detail by comparing with the other two reference materials, bulk Yb_2O_3 and ytterbium chloride ($YbCl_3$). The distribution and biotransformation of the three materials in the roots of cucumbers were observed by TEM and EDS, and were confirmed by STXM coupled with NEXAFS. Possible involved mechanisms for the phytotoxicity of Yb_2O_3 NPs will be discussed.

MATERIALS AND METHODS

Preparation and Characterization of Yb_2O_3 Particles. Ytterbium oxide nanoparticles were synthesized using a precipitation method as previously described.[11] Bulk Yb_2O_3 were purchased from Sinopharm Chemical Reagent Beijing Co., Ltd. (China), with a purity of 99.99%. The characterization of nano- and bulk-Yb_2O_3 is described in detail in the Supporting Information (SI).

Root Elongation. Cucumber (*Cucumis sativus*) is a widely consumed crop plant, with high economical and ecological relevance, and recommended for use in phytotoxicity studies by U.S. EPA.[27] Seeds germination and growth were described in the SI. For the root elongation experiments, the seeds were treated with sterile ultrapure water or different concentrations (0.32, 0.8, 2, 5, 20, 200, 2000 mg/L) of nano-, bulk-Yb_2O_3 suspensions, or $YbCl_3{\cdot}6H_2O$ solution, respectively. Nano- and bulk-Yb_2O_3 were added into the ultrapure water followed by ultrasonic treatment (100 W, 40 kHz) for 30 min before being planted. Exposure to Yb^{3+} ion were obtained by dissolving $YbCl_3{\cdot}6H_2O$ in water. The highest concentration was selected to investigate if these materials were toxic to the test plant (cucumber in this study) according to the U.S. EPA guidelines.[27] After 5 days, the germination was halted and seedling root lengths were measured by a millimeter ruler.

Biomass and Yb Concentration Determination. The seedlings at the second leaf stage were allowed for the biomass study. Growth conditions are described in the SI. Since the solubility of REE phosphate is extremely low,[28] 1 mM KH_2PO_4 in the nutrient solution were replaced by 0.25 mM KCl to avoid the precipitation. This solution was called -P nutrient solution. In addition, 1 mM KH_2PO_4 was sprayed on foliage every other day to apply requisite inorganic phosphate for plants. Four separate treatments were performed as follows: control (-P nutrient solution without adding Yb_2O_3 particles or $YbCl_3$) and seven concentrations (0.32, 0.8, 2, 5, 20, 200, 2000 mg/L) of nano-, bulk-Yb_2O_3 or $YbCl_3{\cdot}6H_2O$, respectively. All concentrations of treatments were performed with eight seedlings each. The pH values of nutrient solution were changed from 5.5 to around 7.0 after addition of 2000 mg/L Yb_2O_3 particles. The test medium was replenished with nutrient solution to the constant volume (100 mL) every the other day. The experiment lasted for 14 days. On the last day, free Yb^{3+} ion concentrations in the supernatants of all the exposure solutions in situ with the plants growing in them were determined by a colormetric method[29] (SI). Yb^{3+} ion concentrations in the rhizosphere solutions[13] were also measured on the last day.

At the end of experiment, the seedlings were thoroughly washed with flowing tap water and ultrapure water, successively. Roots and shoots were separated, and their biomass was measured after drying to a constant weight at 75 °C. The dry samples were ground to fine powders by the agate mortar and pestle. Each sample with an amount of 10 mg of root, 20 mg of shoot, or 10 mg of standard reference material (bush branches and leaves, GBW 07602) was digested with the mixture of 1.2 mL HNO_3 and 0.3 mL H_2O_2 in a 15 mL digestion vessel using the Mars Xpress Microwave Digestion System (CEM, USA). The residue was dissolved with ultrapure water and transferred into a 10 mL flask, and then diluted to the specific volume. Total Yb contents in cucumber tissues were determined by ICP-MS (Thermo, U.S.). Indium (20 ng/mL) was added in the solution as an internal standard to compensate for matrix suppression and signal drifting. Analytical runs included calibration verification samples, spike recovery samples, and duplicate dilutions. Mean recovery of Yb from GBW 07602 was 104%. Spike recovery averaged 102%, and the mean relative percent difference between replicate samples was 3%. The range of linearity was 0.1 to 50 ng/mL, and the lower limit of quantitation is 0.1 ng/mL. The detection limit is 0.003 ng/mL.

Microscopy Observations and Energy-Dispersive Spectroscopy (EDS). Fresh cucumber roots were thoroughly washed with ultrapure water. The main root samples were collected and prefixed in 2.5% glutaraldehyde in 0.1 M phosphate buffered saline (PBS, pH 7.2), washed with PBS three times, and postfixed in 1% osmium tetroxide for 1 h. Then, the samples were dehydrated in a graded acetone series and embedded in Spurr's resin. In order to eliminate the possibility that the phosphate deposits were formed during the sample preparation process, we performed the fixation in PBS or HEPS buffer separately and compared the results. The almost identical TEM images under these two conditions verified that the embedding procedure did not change the state of Yb in samples (Figure S6 of the SI). The cell morphology of the root tips under the control and three types of treatments was observed with a light microscopy (LM, Olympus, Japan). The first 2 mm root tips were longitudinally sliced (700-nm thick) and stained with 0.05% toluidine blue in 0.5% sodium

borate for LM. For TEM and EDS, the ultrathin (90-nm thick) cross sections were obtained and observed with similar methods to those described in our previous work.[30]

STXM. STXM imaging and M-edge NEXAFS measurements of Yb were performed at the beamline BL08U1 of the Shanghai Synchrotron Radiation Facility (SSRF). Samples of root sections with a thickness of 1 μm were prepared by the protocol as used in the TEM experiment. Besides Yb_2O_3, $YbPO_4$, and $Yb(Ac)_3$ (as a representative of compounds containing carboxylate) were also chosen as the reference materials. The reference materials were sonically dispersed in ethanol and deposited on a TEM grid. The grid was fixed on a sample holder and loaded into the experimental chamber. Single-energy images at selected energies were scanned and recorded as raw data. The cluster analysis method can be used to obtain not only Yb speciation maps, but also the corresponding NEXAFS spectra. First, sequences of images ("stack") were recorded at a series of energies around the relevant absorption edge (from 1520 to 1538 eV for Yb 3d edge). Then they were aligned via a spatial cross-correlation analysis method. Finally, NEXAFS spectra were extracted from groups of pixels that have similar absorption features within the image region of interest using the IDL package aXis2000. At least three root sections from different seedlings per treatment were examined by LM, TEM, and STXM.

Data Analysis. The results were expressed as mean ± SD (standard deviation). One-Way ANOVA followed by Tukey's HSD (equal group size) or Bonferroni (unequal group size) test was employed to examine the statistical differences. $P < 0.05$ was considered to be a significant difference. All statistical analyses were conducted using Statistical Packages for the Social Sciences (SPSS) Version 15.0.

RESULTS AND DISCUSSION

Characterization of Yb_2O_3 Particles. Typical TEM images show the morphologies of Yb_2O_3 particles in ultrapure water (Figure S1 of the SI). The shape of pristine nano-Yb_2O_3 was sphere-like with clear crystal lattices. Most of the bulk-Yb_2O_3 particles are larger than 200 nm, with a few particles smaller than 100 nm. The detailed physicochemical properties of two-sized Yb_2O_3 particles are shown in Table 1. Both kinds of particles were free of other heavy metal impurities. The larger mean diameters of Yb_2O_3 particles in ultrapure water and -P nutrient solution implied that agglomerations had occurred in the media. After being incubated in ultrapure water (5 days) or -P nutrient solution (14 days), a small part of Yb_2O_3 particles was dissolved (<1%). Nevertheless, about 10 times or more of Yb_2O_3 particles were dissolved in acetic acid-sodium acetate (HAc-NaAc, pH 5.5) buffer after 14 days, suggesting that the organic acid facilitated the dissolution of particles.

Effects of nano-, bulk-Yb_2O_3, and $YbCl_3$ on root elongation of cucumbers. Concentration-dependent root elongation of cucumber under nano-, bulk Yb_2O_3, and $YbCl_3{\cdot}6H_2O$ treatments are displayed in Figure 1. There appears a concentration threshold of each treatment, below which no significant inhibition was observed. After that, the root elongation decreased rapidly with increasing concentration. The inhibitions were all enhanced under the three treatments when concentrations were higher than 200 mg/L. At the highest concentration of nano-, bulk Yb_2O_3, and $YbCl_3{\cdot}6H_2O$, the root elongations were reduced by 78.1%, 46.9%, and up to 97% with respect to each control, respectively. The EC_{50}, defined as 50% effective concentrations, of

Table 1. Physicochemical Properties of Yb_2O_3 Particles

	nano-Yb_2O_3	bulk-Yb_2O_3
particle size (TEM)[b]	12 ± 2 nm	
crystal form	cubic C-type	cubic C-type
purity	99.7%	99.99%
hydrodynamic mean diameter (DLS)[c] (in ultrapure water)	62 ± 8 nm	≥1 μm
hydrodynamic mean diameter (DLS)[c] (in −P nutrient solution)	146 ± 15 nm	≥1 μm
zeta potential (in ultrapure water)[c]	12.26 mV	26.63 mV
zeta potential (in −P nutrient solution)[c]	−15.23 mV	−26.96 mV
pH value (in −P nutrient solution)[c]	6.6	6.3
The percentage of Yb^{3+} ions in ultrapure water (after 5 days)[d]	0.38 ± 0.03%	0.31 ± 0.02%
percentage of Yb^{3+} ions in −P nutrient solution (after 14 days)[d]	0.93 ± 0.08%	0.75 ± 0.06%
percentage of Yb^{3+} ions in pH 5.5 HAc-NaAc buffer (after 14 days)[d]	12.8 ± 0.9%	7.0 ± 0.4%

[a]The values represent means of 3 replicates ± SD. [b]The mean diameter of nano-Yb_2O_3 was calculated from 72 particles. The diameters of bulk-Yb_2O_3 were nonuniform. [c]The results were measured with 20 mg/L suspensions after sonication for 30 min. [d]The results were measured with 2000 mg/L suspensions.

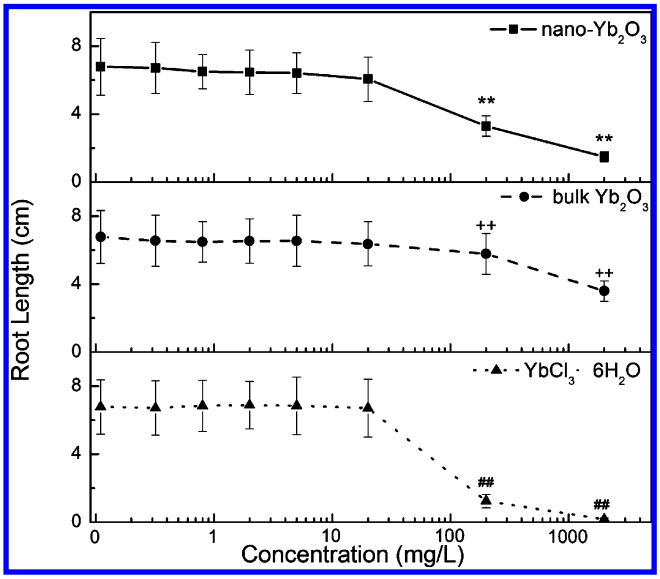

Figure 1. Concentration−response curves of root elongation of cucumber treated with nano-, bulk-Yb_2O_3, or $YbCl_3{\cdot}6H_2O$. The values were given as mean ± SD (standard deviation). Significant differences versus control were marked with"**", "++", and "##" ($p < 0.01$) for nano-, bulk Yb_2O_3, and $YbCl_3{\cdot}6H_2O$ treatments, respectively.

$YbCl_3{\cdot}6H_2O$ was about 78 mg/L (34.8 mg Yb/L), which was lower than that of nano-Yb_2O_3 (182 mg/L, 159.8 mg Yb/L). Yb^{3+} ion appears to be about three times more toxic than Yb_2O_3 NPs in terms of EC_{50} values in this study. Bulk-Yb_2O_3 had least inhibition on root elongation among these three materials.

Effects of Nano-, Bulk-Yb_2O_3, and $YbCl_3$ on Biomass and Total Yb Contents in Cucumbers. Figure 2A shows the concentration−response curves of nano-, bulk-Yb_2O_3, and $YbCl_3{\cdot}6H_2O$ to the cucumber biomass. The cucumber plants were severely harmed by all treatments at concentrations higher than 20 mg/L, indicated by the significant decreases in biomass. For nano-Yb_2O_3, there was significant inhibition of biomass at

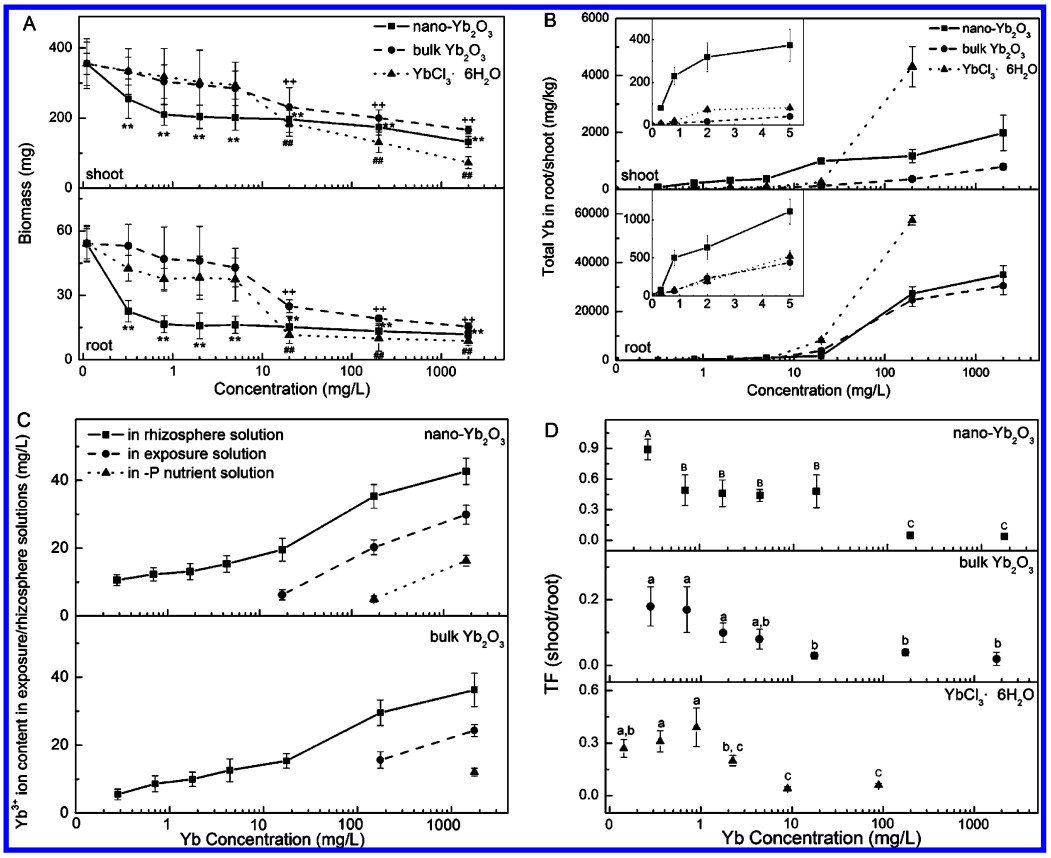

Figure 2. Cucumber biomass reduction (A), root/shoot Yb contents of the seedlings (B), free ions concentration in exposure or rhizosphere solutions (C), and TFs of Yb (D) under the treatments of Yb_2O_3 particles or $YbCl_3{\cdot}6H_2O$. The values were given as mean ± SD. Significant differences versus control in A were marked with "**", "++", and "##" ($p < 0.01$) for nano-, bulk Yb_2O_3, and $YbCl_3{\cdot}6H_2O$ treatments, respectively. The concentrations lower than 1 mg/L in the solutions were not shown in C. The same letters in D were not significantly different from each other and the significant differences were marked with lowercases ($p < 0.05$) or uppercase ($p < 0.01$). At 2000 mg/L of $YbCl_3{\cdot}6H_2O$, the seedlings were almost dead at the end of experiment, so the data in this group were omitted in B and D.

exposure as low as 0.32 mg/L, indicating that this material within the environment would pose a potential risk to higher plants and therefore the ecosystem. At the highest concentration (2000 mg/L) of nano-, bulk-Yb_2O_3, and $YbCl_3{\cdot}6H_2O$, the biomass of roots/shoots were reduced by 78.3%/62.9%, 70.5%/53.2%, and 83.9%/80.5% to the controls, respectively. The inhibition thresholds and degrees at higher concentrations at this stage are both different from those at newly germinated stage, indicating that biomass is a more sensitive biomarker and the susceptibility to toxic compounds of a plant is growth stage-dependent. Moreover, the biomass experiment lasted for 14 days, which was longer than that for the root elongation experiment (5 days). Contacting with the suspensions for a longer time might be another reason for the seedlings being inhibited severely in the biomass experiment. The inhibition of biomass by nano-Yb_2O_3 at 0.32 mg/L for 14 days suggests that NPs need a longer time to affect plant growth, especially at lower concentrations. Thus, the effects of NPs on plant growth may require a longer period of exposure to determine sublethal effects.[31]

The total Yb concentrations in cucumber tissues under three treatments are shown in Figure 2B. As seen in the figure, total Yb contents in roots and shoots increased with the increasing concentrations of compounds in the exposure solutions. The majority of Yb was accumulated in the roots under all treatments. At concentrations less than 5 mg/L, there are steeper rises of Yb contents in roots and shoots under treatment with nano-Yb_2O_3, as shown in the insets of Figure 2B. The inhibition degree of the three materials has a relation to the actual amount of Yb uptake by the cucumber plants (Figure 2A,B). At lower concentrations (≤5 mg/L), much more toxic Yb entered the plants in nano-Yb_2O_3 treatment group, thus the inhibition was more severe than the other two groups. At higher concentrations (≥200 mg/L), the most severe inhibition was induced by $YbCl_3$ with the similar reason. Rhizosphere solutions are mainly composed with mucilage and root exudates, containing large amounts of organic acids and amino acids,[32] which might promote the adsorption of NPs on the root surface and change their properties.[13,33] In this study, Yb^{3+} ion concentrations in the rhizosphere solutions are indeed higher than those in exposure solutions (with the plants growing in them) or in -P nutrient solutions (without plants) (Figue 2C), indicating that the nanobio interface was the main location of dissolution. Because of the enhanced release of Yb^{3+} ions from the particles on the root surface, Yb^{3+} ion concentrations in the exposure solutions were also significantly increased. From these results, it is evident that the interaction of plants and particles improved the dissolution of particles.

It seems that there were significant differences in the transporting behavior among nano-, bulk-Yb_2O_3, and $YbCl_3$ in cucumber plants, which could be evaluated by transfer factors (TFs, defined as Yb content ratio of shoot to root). For comparison, they were normalized to actual Yb concentrations in the exposure solutions at X axis (Figure 2D). Under the

dx.doi.org/10.1021/es2027295 | Environ. Sci. Technol. 2012, 46, 1834–1841

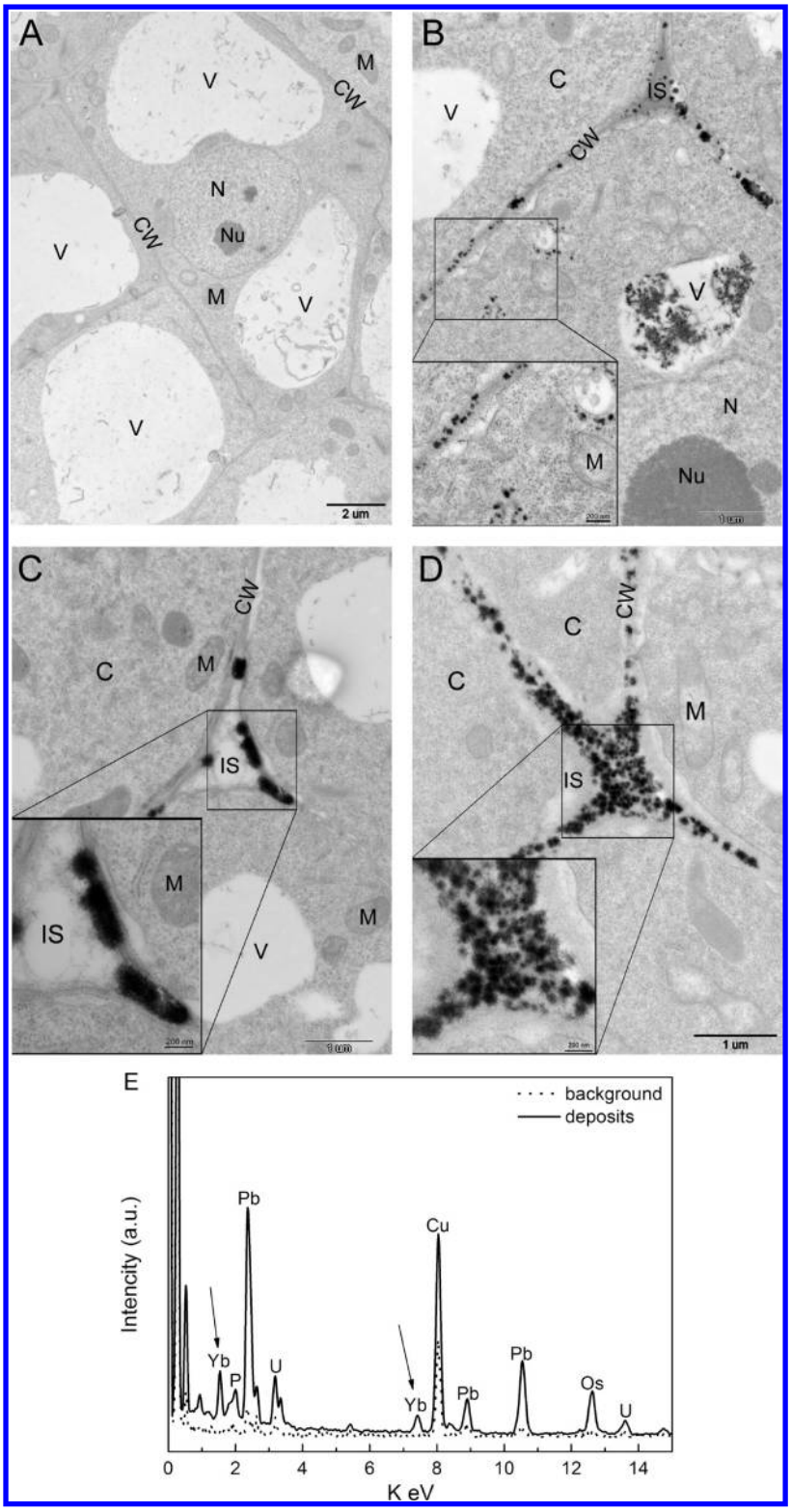

Figure 3. TEM images of cross sections of cucumber root cells under the control (A), 2000 mg/L nm-Yb_2O_3 (B), 2000 mg/L bulk Yb_2O_3 (C), 200 mg/L $YbCl_3$ (D), and representative EDS spectra of background and dense deposits in TEM images (E). The insets are higher magnification of the rectangle areas. Cells walls (CW), nucleus (N) with nucleolus (Nu), intercellular space (IS), mitochondria (M), and vacuole (V).

nano-Yb_2O_3 treatment, the TFs were much higher than those under the other two, especially at the lower concentrations. Given the larger amounts of ions in rhizosphere solutions in Figure 2C, the greater uptake and translocation of NPs might be due to the greater adsorption and interaction with roots. More particles were adsorbed onto the root surface, making higher concentrations in the vicinity of the root. The concentrating effect was distinct at lower exposure concentrations (Figure 2C). The TFs were different under nano- and bulk Yb_2O_3 treatments, although they had the similar adsorption on the root surface. Bulk particles were too large to enter the plant roots while the NPs could, which might result

in the higher uptake and TFs under the latter treatment. It should be noted that the Yb contents of the roots determined by ICP-MS were the total contents, including those adsorbed to the exterior surfaces and taken up by the roots. It was difficult to differentiate Yb inside or outside the root by this method. Our previous study indicated that about 10% of the compact conjoint NPs on the root surface could not be removed by the simple wash with water.[34] Also shown in Figure 2D, the TFs decreased with the concentrations in all treatments and this decrease was the greatest with the nano-Yb_2O_3 treatment at higher exposure concentrations (≥200 mg/L). The adsorption of particles on the root surface might be saturated, so not all of them could get into the roots and the TFs become underestimated to some extent. Moreover, normal functions of the roots were impaired at such high concentrations, so the TFs under this condition could not represent the actual transport behavior of the plants.

Yb Distribution and Spatially Resolved Speciation in the Cucumber Roots. The morphology changes of cucumber roots under the three treatments were examined by LM of the longitudinally sectioned main root tips (SI Figure S3). Toxic symptoms induced by $YbCl_3{\cdot}6H_2O$ were more severe than those induced by nano- or bulk Yb_2O_3 at higher concentrations (>200 mg/L). The shoots became yellow and the seedlings almost died in the presence of 2000 mg/L of $YbCl_3{\cdot}6H_2O$, so the cucumber roots under the treatment of 200 mg/L $YbCl_3{\cdot}6H_2O$ were used in the microscopy observations. TEM images of the cross sections of cucumber roots under the different treatments are shown in Figure 3. In contrast to the thin cell walls in the section of untreated root meristem (Figure 3A), there are thicker cell walls and a lot of high electron-dense deposits in the intercellular spaces and middle lamellas in sections of the three treatment groups (Figure 3B–D). Moreover, these dark deposits look like composed of fine needle-shaped nanoclusters, and the shapes of which are apparently different from those of original Yb_2O_3 particles, neither nano- nor bulk (Figure S1). It is worth noting that there were some dark deposits in the cytoplasm and vacuoles of root cells only under the treatment of nano-Yb_2O_3 (Figure 3B and the inset). The atomic compositions of these electron-dense deposits (including those in the cytoplasm and vacuoles, see SI Figures S4 and S5) were analyzed by EDS spot-scanning technique to confirm the presence of Yb in them. The representative EDS spectra of spots from the background (the area away from the electron dense areas, but still in the tissue) and deposits in the intercellular regions are shown in Figure 3E. The spectrum of the blank background is plain without Yb peak in it, whereas the needle-like nanoclusters contain some concentration of Yb indicated by the presence of Yb peak in the EDS spectrum. The high peaks of Cu, Os, Pb, and U in the spectrum were caused by the background effect of Cu grids, fixation and stain reagents, respectively. Besides, there is also some concentration of P in the deposits and the relative atomic ratios of Yb/P analyzed by the EDS peak areas are close to 1. From this, the composition of the deposits could be deduced to be $YbPO_4$.

Although the possible composition of the precipitates was implied by the signals of Yb and P in the EDS spectra, it was necessary to identify the chemical species of Yb in the cucumber roots. The cross root sections adjacent to those for TEM observations, with a different thickness (ca. 1 μm), were further investigated by STXM. It could not only outline the morphological features of the specimen, but also map the chemical distribution simultaneously.[35] Figure 4A,C shows the spatial distribution of Yb species under the treatment of 2000 mg/L nano-Yb_2O_3 and 200 mg/L $YbCl_3$, repectively. Since the deposits in the root under bulk Yb_2O_3 treatment were very sparse, the STXM result of this group was not shown. The color-coded map displayed the high (red) and low abundance (yellow) of the Yb-containing species areas, and the non-Yb (blue) area. The results of cluster analysis show that there was only one compound with a characteristic split peak at 1530 eV but varying abundances in the intercellular regions. The distribution of Yb obtained by STXM was at similar regions as that from TEM (Figure 3). The Yb inside the cells under nano-Yb_2O_3 treatment was not detected by STXM, which might be due to the lower sensitivity and resolution of STXM than TEM. In Figure 4B,D, the extracted Yb-3d spectra are compared with the spectra of several Yb-containing reference compounds (Yb_2O_3, $Yb(Ac)_3$, and $YbPO_4$). On the basis of the similarity (full width at half-maximum, FWTH) of NEXAFS spectra of the samples with those of the reference materials, this compound can be inferred to be $YbPO_4$. These results are in general agreement with the observations by TEM and EDS, indicating that the TEM image and STXM spectromicroscopy data validate and corroborate each other. Figures 3, 4, and S3 report representative data.

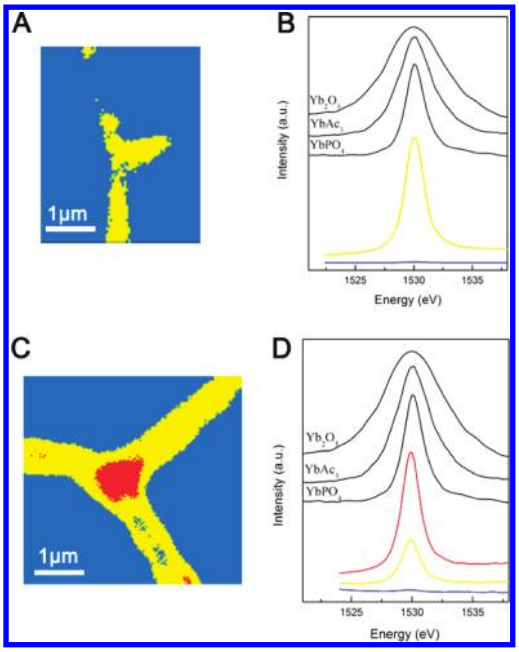

Figure 4. Color-coded composite maps of Yb-component derived from STXM Yb 3d edge stack analysis in cucumber root sections exposed to 2000 mg/L nano-Yb_2O_3 (A) and 200 mg/L $YbCl_3$ (C). Red = high-content Yb regions; Yellow = low-content Yb regions; Blue = non-Yb regions. Yb 3d spectra extracted from the image sequence of A (B) and C (D).

Possible Mechanisms Involved in the Phytotoxicity of Yb_2O_3 Particles. In order to investigate the phytotoxic mechanism of Yb_2O_3 NPs, we compared the distribution of nano-, bulk Yb_2O_3, and $YbCl_3$ in root tissues of cucumber plants. The majority of deposits under nano-Yb_2O_3 treatment, as well as all the deposits under bulk Yb_2O_3 and $YbCl_3$ treatments were adhered to cell wall in the TEM images. In addition, the results clearly showed that nano-, bulk Yb_2O_3 and $YbCl_3$ were all biotransformed into $YbPO_4$ in cucumber roots.

dx.doi.org/10.1021/es2027295 | Environ. Sci. Technol. 2012, 46, 1834–1841

The in situ observation of this morphology change was very similar to that of our previously report about the La_2O_3 NPs and $LaCl_3$ in plants.[30] In this study, we found that Yb^{3+} ion concentrations in the rhizosphere solutions are higher than that in the exposure solutions or -P nutrient solutions (Figure 2C), and the dissolution of particles in the presence of HAc in the in vitro experiment was also promoted (Table 1). Therefore, we hypothesized that the phytotoxicity of Yb_2O_3 particles mainly came from the dissolution and released ions induced by organic acids excreted from the roots.

It should be noted that, besides in the cell walls, insoluble $YbPO_4$ precipitates also appeared in the cytoplasm under the nano-Yb_2O_3 treatment (Figue 3B). But for the other two reference materials, there were no obvious deposits in the cytoplasm, suggesting the different behavior of the three materials in cucumber plants. Similar to lanthanum ions, which have always been used as an electron-dense tracer to delineate the apoplastic pathways in plants,[36] ytterbium ions ($YbCl_3$) in this study were also localized in the cell walls. Our previous studies suggest that NPs might enter plant roots through the apical meristematic tissue below the root cap at the root tip.[34] Nevertheless, the bulk Yb_2O_3 particles might be too large to enter the plant roots. When adsorbed on the root surface, some particles were dissolved at the root surface and transported in roots as ionic form, with similar effects to those of ions. However, there still a part of NPs adsorbed on the meristem region was uptaken by cucumber roots. Some of them might be transported to aerial parts with water and nutrients via transpiration, which brings about the different TFs under NPs from the other two reference materials in cucumber seedlings (Figure 2D). Others might be internalized by root cells,[37,38] and then transformed to $YbPO_4$. Accordingly, the phytotoxicity of nano-Yb_2O_3 appears to be not only from the transformed ions on the root surface, but also from the NPs uptake and biotransformation inside the cells.

■ ASSOCIATED CONTENT

Supporting Information

More details on experimental setup, particle characterization, TEM micrographs of particles and sections, and EDS spectra. This information is available free of charge via the Internet at http://pubs.acs.org.

■ AUTHOR INFORMATION

Corresponding Author

*Tel: +86-10-88233215; fax: +86-10-88235294; e-mail: zhangzhy@ihep.ac.cn.

Author Contributions

†These authors contributed equally to this work.

■ ACKNOWLEDGMENTS

This work was financially supported by the Ministry of Science and Technology of China (Grant No. 2011CB933400), Ministry of Environmental Protection of China (Grant No. 201209012), and National Natural Science Foundation of China (Grant No. 10875136, 10905062, 11005118).

■ REFERENCES

(1) Nel, A.; Xia, T.; Madler, L.; Li, N. Toxic potential of materials at the nanolevel. *Science* **2006**, *311* (5761), 622−627.

(2) Oberdörster, G.; Oberdörster, E.; Oberdörster, J. Nanotoxicology: An emerging discipline evolving from studies of ultrafine particles. *Environ. Health Perspect.* **2005**, *113*, 823−839.

(3) Maynard, A. D.; Aitken, R. J.; Butz, T.; Colvin, V.; Donaldson, K.; Oberdorster, G.; Philbert, M. A.; Ryan, J.; Seaton, A.; Stone, V.; Tinkle, S. S.; Tran, L.; Walker, N. J.; Warheit, D. B. Safe handling of nanotechnology. *Nature* **2006**, *444* (7117), 267−269.

(4) Zhao, Y.; Xing, G.; Chai, Z. Nanotoxicology: Are carbon nanotubes safe? *Nat. Nanotechnol.* **2008**, *3* (4), 191−192.

(5) Zhu, H.; Han, J.; Xiao, J.; Jin, Y. Uptake, translocation, and accumulation of manufactured iron oxide nanoparticles by pumpkin plants. *J. Environ. Monit.* **2008**, *10* (6), 713−717.

(6) Holbrook, R.; Murphy, K.; Morrow, J.; Cole, K. Trophic transfer of nanoparticles in a simplified invertebrate food web. *Nat. Nanotechnol.* **2008**, *3* (6), 352−355.

(7) Judy, J. D.; Unrine, J. M.; Bertsch, P. M. Evidence for biomagnification of gold nanoparticles within a terrestrial food chain. *Environ. Sci. Technol.* **2011**, *45*, 776−781.

(8) Lin, D.; Xing, B. Phytotoxicity of nanoparticles: Inhibition of seed germination and root growth. *Environ. Pollut.* **2007**, *150* (2), 243−250.

(9) Lee, W.; An, Y.; Yoon, H.; Kweon, H. Toxicity and bioavailability of copper nanoparticles to the terrestrial plants mung bean (*Phaseolus radiatus*) and wheat (*Triticum aestivum*): Plant agar teat for water-insoluble nanoparticles. *Environ. Toxicol. Chem.* **2008**, *27* (9), 1915−1921.

(10) Barrena, R.; Casals, E.; Colón, J.; Font, X.; Sánchez, A.; Puntes, V. Evaluation of the ecotoxicity of model nanoparticles. *Chemosphere* **2009**, *75* (7), 850−857.

(11) Ma, Y.; Kuang, L.; He, X.; Bai, W.; Ding, Y.; Zhang, Z.; Zhao, Y.; Chai, Z. Effects of rare earth oxide nanoparticles on root elongation of plants. *Chemosphere* **2010**, *78* (3), 273−279.

(12) Franklin, N.; Rogers, N.; Apte, S.; Batley, G.; Gadd, G.; Casey, P. Comparative toxicity of nanoparticulate ZnO, bulk ZnO, and $ZnCl_2$ to a freshwater microalga (*Pseudokirchneriella subcapitata*): The importance of particle solubility. *Environ. Sci. Technol.* **2007**, *41* (24), 8484−8490.

(13) Lin, D.; Xing, B. Root uptake and phytotoxicity of ZnO nanoparticles. *Environ. Sci. Technol.* **2008**, *42* (15), 5580−5585.

(14) Navarro, E.; Piccapietra, F.; Wagner, B.; Marconi, F.; Kaegi, R.; Odzak, N.; Sigg, L.; Behra, R. Toxicity of silver nanoparticles to *Chlamydomonas reinhardtii*. *Environ. Sci. Technol.* **2008**, *42* (23), 8959−8964.

(15) Stampoulis, D.; Sinha, S.; White, J. Assay-dependent phytotoxicity of nanoparticles to plants. *Environ. Sci. Technol.* **2009**, *43* (24), 9473−9479.

(16) Xia, T.; Kovochich, M.; Liong, M.; Ma dler, L.; Gilbert, B.; Shi, H.; Yeh, J.; Zink, J.; Nel, A. Comparison of the mechanism of toxicity of zinc oxide and cerium oxide nanoparticles based on dissolution and oxidative stress properties. *ACS Nano* **2008**, *2* (10), 2121−2134.

(17) Theng, B. K. G.; Yuan, G. Nanoparticles in the soil environment. *Elements* **2008**, *4* (6), 395−399.

(18) Unrine, J. M.; Tsyusko, O. V.; Hunyadi, S. E.; Judy, J. D.; Bertsch, P. M. Effects of particle size on chemical speciation and bioavailability of copper to earthworms (*Eisenia fetida*) exposed to copper nanoparticles. *J. Environ. Qual.* **2011**, *39* (6), 1942−1953.

(19) Hussain, S.; Braydich-Stolle, L.; Schrand, A.; Murdock, R.; Yu, K.; Mattie, D.; Schlager, J.; Terrones, M. Toxicity evaluation for safe use of nanomaterials: Recent achievements and technical challenges. *Adv. Mater.* **2009**, *21* (16), 1549−1559.

(20) Lopez-Moreno, M.; de la Rosa, G.; Herna ndez-Viezcas, J.; Castillo-Michel, H.; Botez, C.; Peralta-Videa, J.; Gardea-Torresdey, J. Evidence of the differential biotransformation and genotoxicity of ZnO and CeO_2 nanoparticles on Soybean (*Glycine max*) Plants. *Environ. Sci. Technol.* **2010**, *44* (19), 7315−7320.

(21) Parsons, J.; Lopez, M.; Gonzalez, C.; Peralta-Videa, J.; Gardea-Torresdey, J. Toxicity and biotransformation of uncoated and coated nickel hydroxide nanoparticles on mesquite plants. *Environ. Toxicol. Chem.* **2010**, *29* (5), 1146−1154.

(22) Yoon, T. H. Applications of soft X-ray spectromicroscopy in material and environmental sciences. *Appl. Spectrosc. Rev.* **2009**, *44* (2), 91−122.

(23) Obst, M.; Dynes, J. J.; Lawrence, J. R.; Swerhone, G. D. W.; Benzerara, K.; Karunakaran, C.; Kaznatcheev, K.; Tyliszczak, T.; Hitchcock, A. P. Precipitation of amorphous $CaCO_3$ (aragonite-like) by cyanobacteria: A STXM study of the influence of EPS on the nucleation process. *Geochim. Cosmochim. Acta* **2009**, *73* (14), 4180–4198.
(24) Patil, S.; Kuiry, S.; Seal, S.; Vanfleet, R. Synthesis of nanocrystalline ceria particles for high temperature oxidation resistant coating. *J. Nanopart. Res.* **2002**, *4* (5), 433–438.
(25) Gordon, W.; Carter, J.; Tissue, B. Long-lifetime luminescence of lanthanide-doped gadolinium oxide nanoparticles for immunoassays. *J. Lumin.* **2004**, *108*, 339–342.
(26) Yada, M.; Mihara, M.; Mouri, S.; Kuroki, M.; Kijima, T. Rare Earth (Er, Tm, Yb, Lu) oxide nanotubes templated by dodecylsulfate assemblies. *Adv. Mater.* **2002**, *14* (4), 309–313.
(27) Environmental Protection Agency. Ecological effects test guidelines. OPPTS 850.4150 Terrestrial Plant Toxicity, Tier I (vegetative Vigor). EPA 712-C-96–163. Public Draft. Office of Prevention, Pesticides and Toxic Substances, Washington, DC. 1996.
(28) Byrne, R.; Kim, K. Rare earth precipitation and coprecipitation behavior: The limiting role of PO_4^{3-} on dissolved rare earth concentrations in seawater. *Geochim. Cosmochim. Acta* **1993**, *57* (3), 519–526.
(29) Fan, F., Improvement of the method for rapid separation of rare earth elements in ores. *Rock Miner. Anal.* **2000**, *19*, 217-220 (in Chinese).
(30) Ma, Y.; He, X.; Zhang, P.; Zhang, Z.; Guo, Z.; Tai, R.; Xu, Z.; Zhang, L.; Ding, Y.; Zhao, Y. Phytotoxicity and biotransformation of La_2O_3 nanoparticles in a terrestrial plant cucumber (*Cucumis sativus*). *Nanotoxicology* **2010**, *5* (4), 743–753.
(31) Gubbins, E. J.; Batty, L. C.; Lead, J. R. Phytotoxicity of silver nanoparticles to *Lemna minor* L. *Environ. Pollut.* **2011**, *159* (6), 1551–1559.
(32) Bais, H. P.; Weir, T. L.; Perry, L. G.; Gilroy, S.; Vivanco, J. M. The role of root exudates in rhizosphere interactions with plants and other organisms. *Annu. Rev. Plant Biol.* **2006**, *57*, 233–266.
(33) Cañas, J.; Long, M.; Nations, S.; Vadan, R.; Dai, L.; Luo, M.; Ambikapathi, R.; Lee, E.; Olszyk, D. Effects of functionalized and nonfunctionalized single-walled carbon nanotubes on root elongation of select crop species. *Environ. Toxicol. Chem.* **2008**, *27* (9), 1922–31.
(34) Zhang, Z.; He, X.; Zhang, H.; Ma, Y.; Zhang, P.; Ding, Y.; Zhao, Y. Uptake and distribution of ceria nanoparticles in cucumber plants. *Metallomics* **2011**, *3*, 816–822.
(35) Hunter, R.; Hitchcock, A.; Dynes, J.; Obst, M.; Beveridge, T. Mapping the speciation of iron in Pseudomonas aeruginosa biofilms using scanning transmission X-ray microscopy. *Environ. Sci. Technol.* **2008**, *42* (23), 8766–8772.
(36) Lehmann, H.; Stelzer, R.; Holzamer, S.; Kunz, U.; Gierth, M. Analytical electron microscopical investigations on the apoplastic pathways of lanthanum transport in barley roots. *Planta* **2000**, *211* (6), 816–822.
(37) Etxeberria, E.; Gonzalez, P.; Baroja-Fernandez, E.; Romero, J. Fluid Phase endocytic uptake of artificial nano-spheres and fluorescent quantum dots by sycamore cultured cells: evidence for the distribution of solutes to different intracellular compartments. *Plant Signal. Behav.* **2006**, *1* (4), 196–200.
(38) Chen, R.; Ratnikova, T.; Stone, M.; Lin, S.; Lard, M.; Huang, G.; Hudson, J.; Ke, P. Differential uptake of carbon nanoparticles by plant and mammalian cells. *Small* **2010**, *6* (5), 612–617.